RSC Advances

ROYAL SOCIETY OF CHEMISTRY

www.rsc.org/advances

RSC Advances

RSCPublishing

ARTICLE

Preparation and characterization of activated montmorillonite clay supported 11-molybdo-vanado-phosphoric acid for cyclohexene oxidation

Cite this: DOI:

Received,
Accepted

DOI:

www.rsc.org/

S. Boudjema[a], E. Vispe[b], A. Choukchou-Braham[a]*, J.A. Mayoral[b], R. Bachir[a], J.M. Fraile[b]

A new heterogeneous catalyst (PVMo/Bentonite), consisting of vanadium substituted polyphosphomolybdate with Keggin structure $H_4[PVMo_{11}O_{40}].13H_2O$ (PVMo) supported on acid activated Bentonite (clay from Hammam Boughrara, Maghnia, Algeria), was prepared by witness impregnation and characterized by X-ray diffraction, BET, Fourier-transformed infrared spectroscopy, ^{31}P NMR, UV–vis diffuse reflectance spectroscopy and thermogravimetric & differential thermal analysis (TG–DTA). X-ray diffraction indicated that PVMo was properly loaded on Bentonite as a support. Heterogenization of homogenous catalysts is really interesting, as heterogeneous catalysts are recoverable. Therefore, the synthesized materials can be used as efficient heterogeneous catalysts for epoxidation of cyclohexene. The obtained results showed that a better catalytic activity can be obtained with PVMo/Bentonite (81.5 % of conversion), by drop addition of H_2O_2, for 3 hours.

Introduction

The selective catalytic oxidation of organic compounds with a "green" oxidant, such as aqueous H_2O_2, is highly desirable. As cyclohexene is industrially obtained by hydrogenation of benzene by Asahi Kasei corporation [1], and because cyclohexene (CyH) oxidation leads to cyclohexene oxide, followed by epoxide ring-opening and a subsequent oxidation of *trans*-cyclohexane-1,2-diol; this can be a possible route to adipic acid [2-4]. The epoxidation of cyclohexene, using polyoxometalates (in a homogeneous medium) as catalysts and the aqueous hydrogen peroxide as oxidant, was extensively studied [5-11].

Polyoxometalates (POMs) are early transition metal–oxygen anion clusters that exhibit a variety of structures in chemical composition and architecture. Among various POM structural classes, the Keggin-type POMs occupy an important place in the research domain. In the solid state, POMs are ionic crystals consisting of large polyanions, $[XM_{12}O_{40}]^{n-}$ (X = P, Si ... and M = W, Mo), counter-cations (protons, alkalines, transition metals, ammonium salts ...) and crystallization water. The acids corresponding to POMs, namely heteropolyacids(HPAs), are known to possess a Brønsted acidity which is stronger than that of many mineral acids or conventional acidic solids; indeed, they can display a strong oxidative power. For these reasons, these clusters are widely investigated, to see whether they can be used as catalysts in reactions requiring both acidic and oxidative conditions; these reactions can be performed in homogeneous as well as heterogeneous systems [12-16].

Vanadium incorporated molybdophosphoric acid (PVMo) catalysts show unique catalytic features for oxidation due to their bifunctional character which arises from the redox nature of vanadium and the oxidative/acidic character of molybdophosphoric acid [17]. Several authors have investigated V incorporated molybdophosphoric acid catalysts by replacing 1–3 Mo atoms by the corresponding number of V atoms [18, 19]. The acidic, redox and thermal stability properties of PVMo catalysts are influenced by the degree of V substitution [20]. However, owing to their small surface area (< 10 m^2 g^{-1}) and separation problems from the reaction mixture, their catalytic performances are often limited to heterogeneous catalysis [21]. For that reason, several authors proposed to disperse them on porous supports with large surface areas to make the active sites of HPAs more accessible to reactants. The deposition of the modified HPAs on supports is important to increase the surface area. It is always advantageous to use supports like silica, ZrO_2, active carbon, SBA-15, and zeolite, etc... [22-27].

The synergism of clay minerals and heteropolyacids was discussed for the development of many green processes with

[a] *Laboratoire de Catalyse et Synthèse en Chimie Organique, Faculté des Sciences, Université de Tlemcen, Algeria. mail : (* cba@mail.univ-tlemcen.dz)*
[b] *Departamento de Química Orgánica, Instituto de Síntesis Química y Catálisis Homogénea, Facultad de Ciencias, Universidad de Zaragoza-CSIC, Pedro Cerbuna, 12, E-50009 Zaragoza, Spain.*

potential industrial applications [28]. Acid modified clay minerals can also be used as efficient supports [29] because they exhibit higher surface area, pore volume, pore diameter and higher surface acidity [30]; this gives them better adsorption and catalytic properties. In particular, acid treated clay catalysts have received considerable attention in different organic syntheses, as catalysts or as supports, because of their environmental compatibility, low cost and simplicity of use. Using clay catalysts, we can conduct environmentally benign green chemistry both at industrial level and at a laboratory scale. The acid strength of HPA, supported on some of the materials mentioned above, is lower than that of bulk HPA; this is due to the interaction of HPA with surface functional groups of supports. In the case of a composite material, the support has an influence on the acidity function of HPA and vice versa [31]. Acid-treated Montmorillonite exhibits relatively strong acid sites [32]. Several research groups have reported the use of activated clay-supported HPA (e.g., 12-tungstophosphoric acid) in the etherification of phenethyl alcohol with alkanols [33], synthesis of 1,5-benzodiazepine derivatives both in solution and under solvent-free conditions [34], etherification of acetic acid with sec-butanol [29, 35], and hydroxyl alkylation of phenol, respectively. Beside HPA, many metals or metal oxides can be strategically supported on activated clay, metal oxide pillared interlayer clays (PILCs), and porous clay heterostructures (PCHs) as catalysts for organic synthesis [36, 37].

In the present study, we report that HPA like 1-vanado-11-molybdophosphoric acid (PVMo) is supported on acid-activated Montorillonite clay having high surface area, prepared from Montmorillonite by HCl acid activation; it is also considered as a solid acid catalyst for the epoxidation of cyclohexene, using hydrogen peroxide as an oxidant. There are various reasons for choosing this reaction as a model from a wide variety of acid catalyzed and oxidation reactions. Cyclohexene epoxidation is attracting both academic and industrial interest in homogeneous and heterogenous systems [5, 8, 9, 38-49]. Cyclohexene epoxide is a valuable organic intermediate, used in the synthesis of products such as chiral pharmaceuticals, pesticides, epoxy paints, rubber promoters, dyestuffs, plant-protection agents and stabilizers for chlorinated hydrocarbons [43, 47-51]. Again, HPA supported on clay is never used in this reaction. The active centers, responsible for the reactions, are discussed in detail in the manuscript.

2 Experimental

2.1 Catalyst preparation

The synthesis of 1-vanado-11-molybdophosphoric acid, $H_4[PVMo_{11}O_{40}].13H_2O$ (PVMo) was carried out according to the reported method [52].

Raw clay (Montmorillonite) [Hammam Boughrara (Roussel quarry), Algeria] containing silica sand, iron oxide, etc... was purified by a standard sedimentation method to collect the < 2 µm fraction before use.
The purified clay (1 g) was refluxed with 1 M HCl acid (100 mL) at 80 °C for 4 h. The slurry was cooled, filtered, washed thoroughly with water and dried in an air oven at 80 °C, for 24 h [53]. The clay samples thus prepared were designated as HMont.
Samples having 10 and 20 % loading of PVMo on HMont were synthesized by means of the incipient wetness impregnation method. A known amount of PVMo was dissolved in water and the hot support (dried at 120 °C in a furnace, for 6 h) was added to the solution. The dispersion was stirred for 24 h at room temperature, and the solvent was evaporated under vacuum. The catalyst was dried at 100 °C for 4 h and then calcined at 250 °C for 4 h. They were all designated as X%PVMo/HMont.

2.2 Characterization of catalysts

The composition and weight percentages of P, Mo, and V in the samples were evaluated by the XRF technique using a Thermo Electron ARL-ADVANT¨XP X-ray fluorescence spectrophotometer. Prior to analysis, the instrument was calibrated against standard samples using the calibration kit (CAL-SS18) provided by thermo Scientific. Quantization was carried out using Thermo Electron UNIQUANT software.

The surface area and porosity were measured at liquid nitrogen temperature, using Quantachrome Instruments (Nova 1000^e). Prior to each adsorption–desorption measurement, the sample was degassed at T = 150 °C for 3 h. The specific surface areas were determined using the BET equation and the microspore volumes by the de Boer's t-method. The α_s plots were used to estimate the microporosity where $\alpha_s = (n/n_s)$ ref (n_s) is the amount adsorbed by the reference solid $(p/p_0 = s)$.

The materials were characterized by X-ray powder diffraction (XRD) using a Rigaku D/max2500 diffractometer with Cu Kα radiation (λ = 1.541874 Å) in the range 2θ = 2° - 70° with a step of 0.02° and an acquisition time of 1 s.

Fourier transform infrared (FTIR) spectra were recorded by an Agilent Technologies Cary 600 series FTIR spectrometer using KBr pellets, under atmospheric conditions. The FTIR spectra were obtained in KBr pellets in the range of 400–4000 cm^{-1}, and all spectra were collected at room temperature with a resolution of 4 cm^{-1}.

^{31}P MAS NMR (161.70 MHz) spectra were measured at room temperature on a Bruker Avance 400 spectrometer, where 85 % H_3PO_4 was used as an external reference.

The UV–vis diffuse reflectance spectra of the samples were collected in a JASCO V-670 UV–Vis spectrophotometer equipped with a Harrick Praying mantis diffuse reflectance accessory. Spectral grade $BaSO_4$ was used as a reference material.

The thermogravimetric and differential thermal analyses (TG–DTA) measurements of representative samples were carried out using a TA instruments 2960 SDT V3 thermal analyzer. The TG–DTA experiments were performed under argon and nitrogen. About 10mg of the sample was heated at a rate of 10 °C min^{-1}. Quartz cells were used as sample holders with α-Al_2O_3 as a reference. The studied temperature range was 25–800 °C.

2.3 Evaluation of catalytic activity

Catalytic epoxidation reactions were performed in a round bottom flask, in an oil bath, under magnetic stirring (800 rpm). Unless otherwise specified, all oxidation reactions were carried out at atmospheric pressure under reflux with 30 mmol of cyclohexene; 60 % H_2O_2 (30 mmol) was used as oxidant and was slowly added (3 h) with a syringe pump, 10 mL of acetonitrile as solvent, 1 mL of 1,2 dimethoxyethane as internal standard for product quantification, and 25 mg of catalyst. The reaction mixture was stirred at 70 °C. The catalytic reactions were monitored using gas chromatography (Agilent Technologies 7890A GC System) equipped with a Phenomenex Zebron-HT-5

Inferno (30 m x 0.25mm 0.25 µm) column; a flame ionization detector (FID) was also used.
The conversion, product selectivity and product yield were calculated as follows:

$$Conversion\ (\%) = 100 \times \frac{[C_6H_{10}]_0 - [C_6H_{10}]_t}{[C_6H_{10}]_0}$$

$$Selectivity\ (\%) = 100 \times \frac{moles\ of\ individual\ product}{moles\ of\ total\ products}$$

3 Results and discussion

3.1 Characterization

3.1.1. Chemical analysis (XRF)

The results of chemical analysis of heteropolyacids (Table 1) were adjusted considering 11 atoms of molybdenum per Keggin unit, according to the nature of HPA, and were found to be in good agreement with the desired stoichiometry for phosphorous, molybdenum and vanadium. The highest proportions of SiO_2 and Al_2O_3 agree with the nature of the clay support. Moreover, for the impregnated samples, the initial Si, P, Mo and V amounts in PVMo/HMont were found again (within 1 wt.% experimental errors) at the end. Referring to the Mo/P and V/P ratios, average values of 11 and 1, respectively, were obtained for all three preparations, indicating that the quantities of metals used were preserved in the three supported samples.

3.1.2. Surface area and porosity

The surface area and pore volume of HMont and PVMo loaded HMont were measured. It appeared that, in general, the surface area and pore volume of HMont decreased considerably upon loading with PVMo. The results of a typical example, i.e. PVMo/HMont catalysts, are given in Table 2. The surface area (195 $m^2\ g^{-1}$) and the total pore volume of HMont decreased as the amount of PVMo loading increased. Thus, for 20%PVMo loading, the surface area fell to 141 $m^2\ g^{-1}$ and the total pore volume to 0.17 $cm^3\ g^{-1}$ only. The high surface area of acid activated clay was due to the removal of aluminum from the octahedral sites in the clay sheet.

The reduction in surface area and pore volume upon PVMo loading might be due to the blockage of pores by PVMo molecules. These observations suggest that the Keggin units do not penetrate inside the pores but rather stay outside of the surface of the support. Although, in most investigations, the authors considered that HPA can enter into the pores of the support [14, 54, 55], we believe that these conclusions do not take into account the question of anion–anion repulsion and the chemical interaction between the support and HPA protons that could affect the final location of HPA in or on the support.

The complete adsorption–desorption isotherms of calcined samples, are presented in Fig. 1(A). All the curves are nearly similar and can be included in type IV in the BDDT classification. The hysteresis loops, at low pressure, indicate the presence of microspores[56-58]. Assuming the pores to be cylindrical, the average pore radius can be calculated using the formula $r = 2\ V_P / S_p$, where r is the average pore radius, V_p is the pore volume, and S_p is the specific internal surface area of the pores. The average pore radius calculated by this method is reported in Table 2. This shows that with the increase in % loading of PVMo, the average pore radius increases. It is interesting to note that the pore size distribution, determined from the desorption branch of the N_2 adsorption isother using the Barrett–Joyner–Halenda (BJH) method (Fig. 1B), shows that the average pore sizes of different weight percents of PVMo on HMont are in the microporous region.

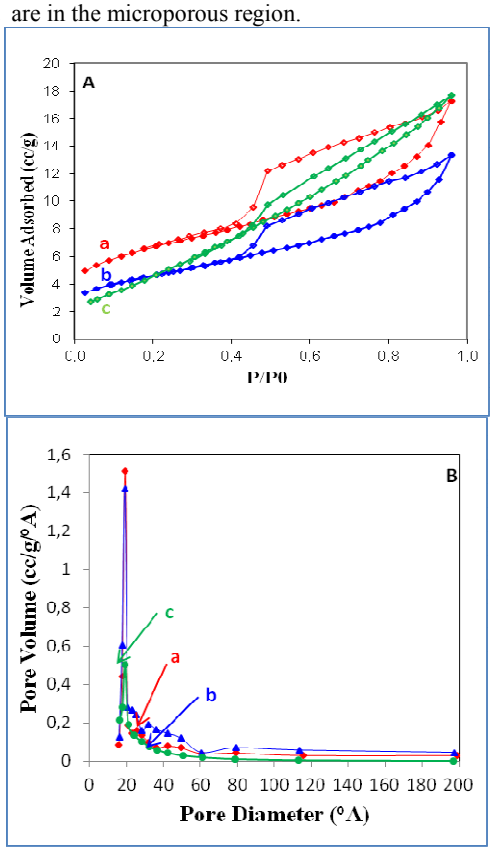

Fig. 1 (A) N_2 adsorption–desorption isotherms. **(B)** Pore size distribution curves of different samples determined by the BJH method.
20%PVMo/HMont b- 10%PVMo/HMont c- HMont

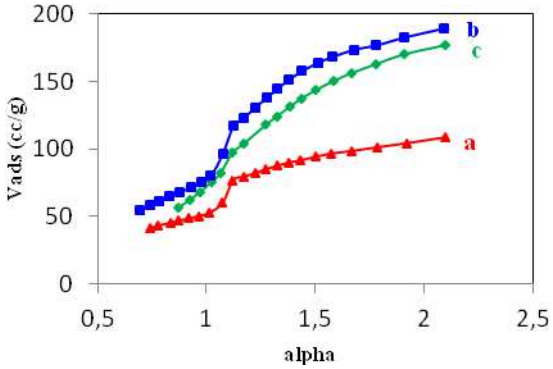

Fig. 2 α_s-plots for (a) 20% PVMo/HMont, (b) 10% PVMo/HMont and (c) HMont

Table 1 Chemical composition of catalysts from XRF

sample	Contents (wt %)										
	SiO_2	Al_2O_3	Fe_2O_3	CaO	MgO	Na_2O	K_2O	TiO_2	P[a]	Mo[a]	V[a]
PVMo	-	-	-	-	-	-	-	-	0.99	11.00	1.00
HMont	57.12	19.87	2.62	0.43	3.10	0.30	2.70	0.24	-	-	-
10%PVMo/HMont	55.31	22.20	2.64	0.01	1.80	0.09	3.28	0.24	0.98	11.00	1.00
20%PVMo/HMont	53.82	23.12	2.92	0.01	2.01	0.09	3.00	0.23	1.05	10.99	1.00

[a]These numbers correspond to the numbers of atoms deduced from the raw wt.% found from XRF, as the number of Mo atoms is fixed to 11.

Table2 Textural properties of various samples

Sample	S_{BET} /m^2 g^{-1}	Pore V /cm^3 g^{-1}	V_m /cm^3 g^{-1}	Av. pore radius / Å	d_{001} /Å
HMont	195	0.27	0.007	1.89	1.65
10% PVMo/HMont	162	0.21	0.025	1.93	1.68
20% PVMo/HMont	141	0.17	0.024	1.97	1.73

3.1.3. XRD

The XRD patterns of supports HMont, PVMo, 10 and 20%PVMo/HMont are presented in Fig. 3. The XRD pattern of PVMo shows its principal diffraction angles at 8.1, 8.9, 9.3, 27.8, 28.2, and 28.88° 2θ. This agrees with those reported in the literature [59] and correspond to 13–14 H_2O hydrates, which are stable at room temperature. The PVMo/HMont materials exhibited refraction, which is due to a basal spacing of 1.80 nm. The decrease in intensity of the diffraction peaks, attributed to clays, was already observed on HMont [29], Mont K10 [60] and silica pillared clay [61] in the presence of heteropoly acids. Moreover, no pattern of the PVMo crystal phase, after impregnation of HPA, indicates that HPA is finely dispersed on the HMont surface; PVMo particles are too small and/or too well dispersed and therefore undetectable by XRD.

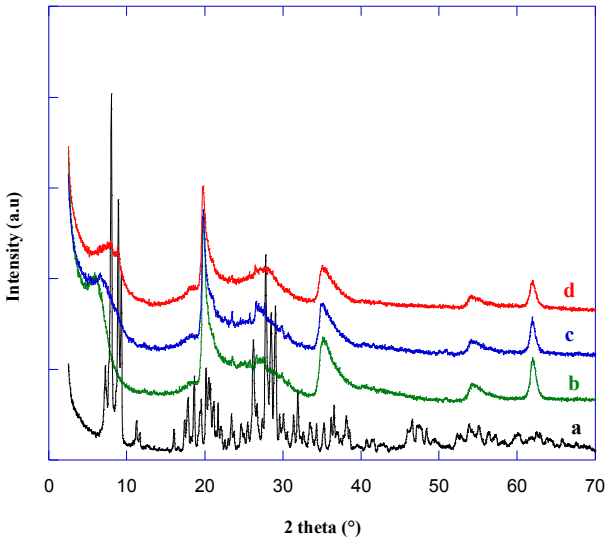

Fig. 3 XRD patterns of (a) PVMo, (b) HMont, (c) 10% PVMo/HMont, (d) 20% PVMo/HMont

3.1.4. FTIR

FTIR spectra of bulk PVMo11, acid activated Montorillonite clay HMont and supported catalysts with 10 and 20 % wt. loadings are shown in Fig. 4. The spectra show a band around 3600 cm^{-1} for all the samples, which is due to asymmetric stretching of OH group. The adsorption band at 1620-1640 cm^{-1} is due to H-O-H bending vibration in water. The IR spectra of a pure sample show bands at 1063, 961, 867 and 780, 596 cm^{-1} that can be attributed to the stretching vibrations of ν_{as} (P–O_a), ν_{as} (Mo–O_d), ν_{as} (Mo–O_b–Mo), ν_{as} (M–O_c–M) (M = Mo, V) and δ(P–Oa) vibrations, respectively. In a Keggin-type unit, O_a refers to the oxygen atom common to PO_4 tetrahedron and one trimetallic group Mo_3O_{13}, O_b connects two trimetallic groups, O_c binds two octahedral MoO_6 units inside a trimetallic group and O_d is the terminal oxygen atom [62, 63]. After the materials were supported on HMont, some of the characteristic Keggin bands were observed at 982 cm^{-1} and 893 cm^{-1} and others merged up with the HMont bands. A decrease in the intensities of these bands was noted as the loading increased.

3.1.5. ^{31}P NMR study

The solid state ^{31}P (MAS) NMR of PVMo is shown in Fig. 5. The ^{31}P chemical shift provides important information about the structure, composition and electronic states of these materials. The ^{31}P NMR spectra of PVMo (Fig. 5) show a chemical shift at - 3.884 ppm; this is in good agreement with the reported one [23, 59, 64].

3.1.6. UV–vis diffuse reflectance spectroscopy

DRUV-Vis spectroscopy provided additional information about the substitution of ions into the Keggin units. The charge transfer absorption spectra of most unreduced polyanions appear in the 200–500 nm range. The acid activated Montorillonite clay, without HPA, displays a characteristic broad band centred at about 245 nm (Fig. 6a) [65, 66].

ARTICLE

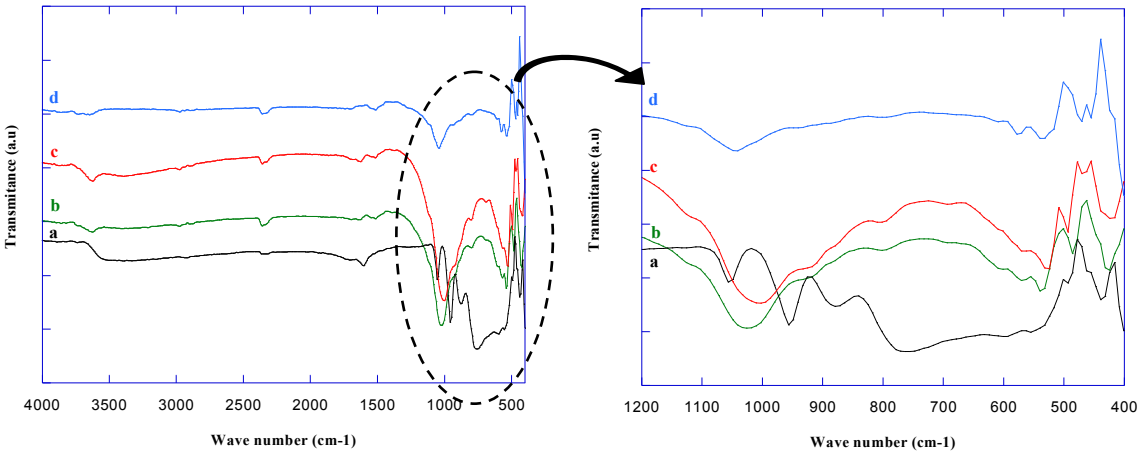

Fig. 4 FTIR spectra of (a) pure PVMo, (b) HMont, (c) 20 % PVMo/HMont, (d) 10 % PVMo/HMont

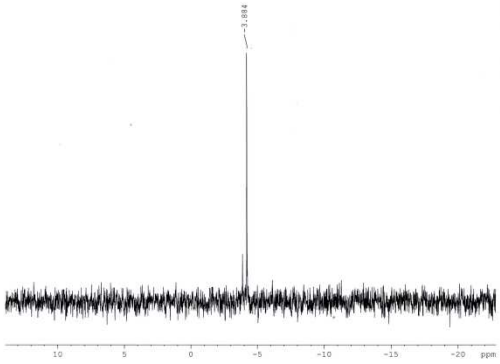

Fig. 5 ^{31}P NMR spectra in D_2O (room temperature) of PVMo

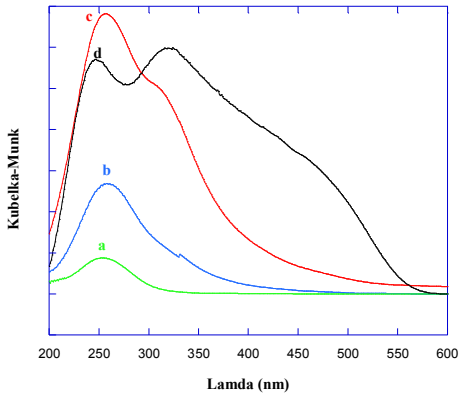

Fig. 6 UV–vis DR spectra of catalysts:

(a) HMont (b) 10% PVMo/HMont (c) 20% PVMo/HMont (d) pure PVMo

This band is assigned to (Fe^{3+}←O^{2-}, OH^- or OH_2) charge transfer band for the iron present in the octahedral layer of the clay mineral. The UV–Vis spectrum of the catalyst (Figs. 6b, 6c) showed absorption maxima at 258 and 308 nm. The 258 nm absorption is typical for the Keggin structure of $H_4PMo_{11}O_{40}$ [28], while the 308 nm shoulder is characteristic of Vanadium incorporation into Keggin ion [1, 51]. These bands are due to ligand-to-metal charge-transfer *(*LMCT*)* transitions associated with octahedrally coordinated Mo^{6+} units [67]. These two absorption bands are clearly seen in the solid-state UV–vis spectra of 20%PVMo, while in the 10%PVMo, the 308 nm band is hardly seen. Since pure HMont (Fig. 6d) shows no UV absorption, then this result confirm the presence of the undegraded primary Keggin structure of PVMo species in 20%PVMo, but suggests a lack of Vanadium substituted HPA species in the case of 10%PVMo.

3.1.7. Differential thermal analysis and thermo gravimetric analysis (DTA/TGA)

The DTA/TGA curves of PVMo, HMont, 10%PVMo/HMont and 20%PVMo/HMont are presented in Fig. 7. Between 50 and 125 °C, DTA shows that all water molecules do not play the same role. In this temperature range, endothermic peaks due to the presence of water molecules interacting in different ways were observed (Fig. 7A). Some of them within clusters, such as H_3O^+ or $H_5O_2^+$, are more tightly bound in the crystal structure. HPA possesses the crystallization water that binds the close Keggin units in the secondary structure by forming water bridges. The weight loss, between 50 and 125 °C, observed in the TGA analyses, indicates that PVMo is hydrated with 13 molecules of water (Fig. 7A). Above ~ 450 °C, DTA shows that HPAs decompose in a mixture of oxides P_2O_5, V_2O_5 and MoO_3 [62, 68].
The DTA/TGA of acid activated clay HMont (Fig. 7B) showed an endothermic signal below 100 °C which represents the dehydration of the smectic structure. A steady loss of mass of about 17 %, up to 500 °C, was attributed to the loss of physisorbed and interlayer water and to the dehydroxylation caused by the breaking of structural OH-groups in the support [30, 69].
The TGA of supported PVMo onto HMont (Figs. 7C and 7D) showed a mass loss of about 18 % within the temperature range of 80 – 150 °C due to a loss of adsorbed water molecules. A gradual mass loss of about 3 %, up to 500 °C, was also observed, which indicates an increase in the thermal stability of PVMo on HMont support. This might be due to the formation of intermolecular bondings between the support and the heteropoly acid; it indicates the presence of a chemical interaction between them [35, 70, 71].

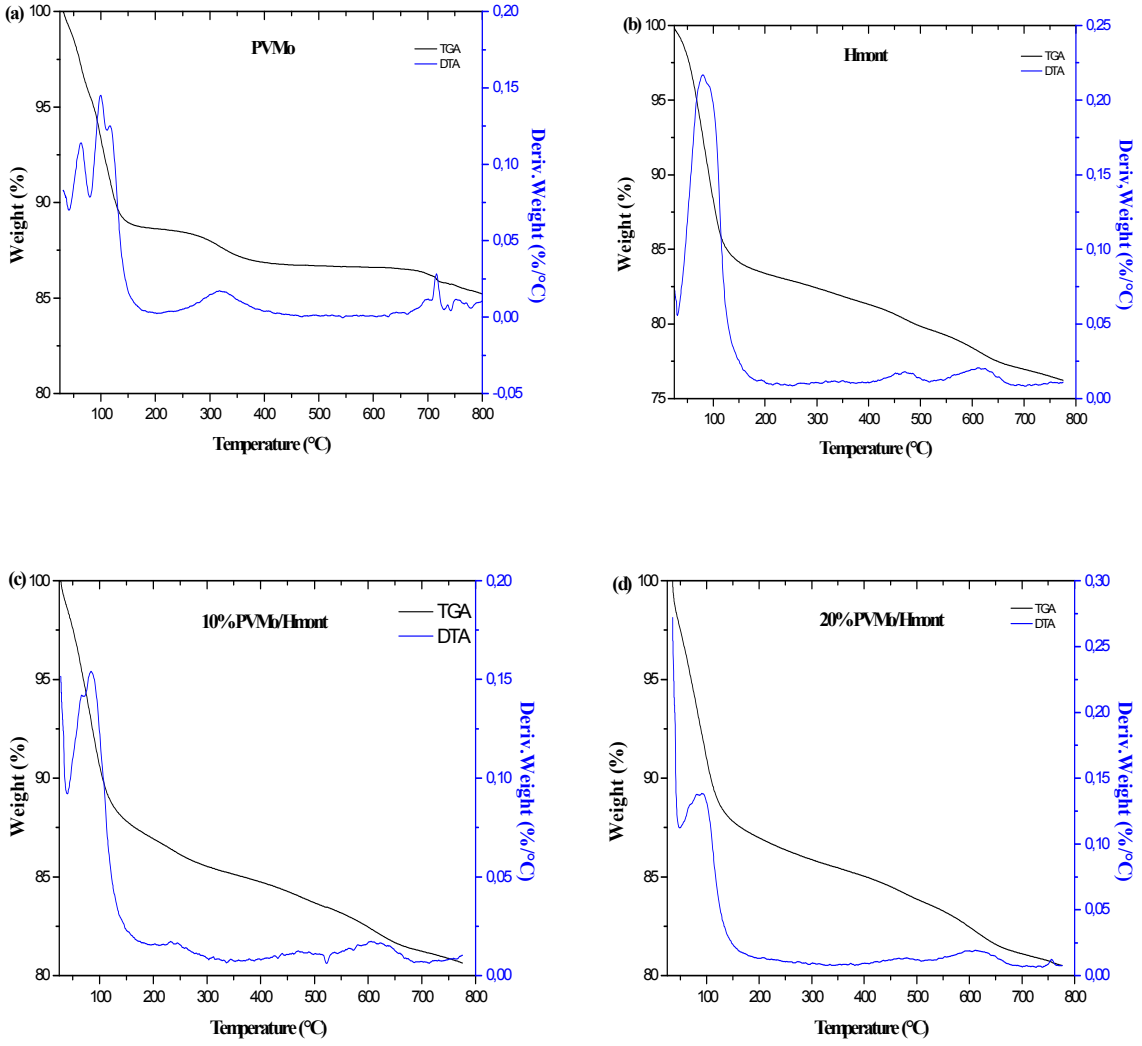

Fig. 7 TGA and DTG curves of (A) PVMo (B) HMont (C) 10%PVMo/HMont (D) 20%PVMo/HMont.

3.2. Epoxidation reaction

Cyclohexene oxidation with H_2O_2 60 % was chosen as a model reaction to compare the behaviours of different catalysts. Cyclohexene epoxidation with alkyl-hydroperoxides mainly yields cyclohexene oxide (epoxide), however when the oxidant is hydrogen peroxide some other products are observed (Fig. 8). *Trans*-1,2-cyclohexanediol is obtained by the acid catalyzed opening of the epoxide with water, small amounts of cyclohexanone (one) can be obtained by the dehydration of this diol with strong acids. Allylic oxidation is a radical process leading to cyclohexene-hydroperoxide, which acts as a secondary oxidant leading to the epoxide and cyclohexenol, furthermore this product dehydrates to yield cyclohexenone, in fact it dehydrates in the injector of the GC so that this amount in the mixture cannot be determined, so the amount on cyclohexenol (enol) and cyclohexenone (enone) determines the contribution of the allylic oxidation. In order to reduce both side-reactions and non-produtive decomposition of the oxidant, a large excess of alkene is used in most of cases, as we want to determine the influence of several parameters in the reaction results we have used equimolecular amounts of both reagents. In order to highlight the impact of heterogeneous catalysts, homogeneous catalytic tests were also achieved. The effects of the nature of H_2O_2, catalyst percentage and reaction time are taken into consideration.
The results show that the way H_2O_2 60 % is added has an impact on conversion (Fig. 9). The best conversion (81.5 %) is reached when hydrogen peroxide is drop-wise added during 3 hours, selectivity to 1-2-diol ids very high (91.6 %) with a small contribution (4.6 %) of allylic oxidation.

The catalytic activities of different samples were evaluated for the oxidation of cyclohexene. All the catalytic systems proved to be highly active and selective towards diol. A blank reaction was performed in the absence of catalyst and no product was detected.

Similar oxidation reactions were also carried out with acid activated montmorillonite support and only a negligible catalytic activity was evidenced, and also no desired product was detected. The obtained results clearly indicate that the POM species are responsible for the high oxidation activity of these heterogeneous catalysts. Besides, the large pores of the HMont support permit diffusion of a relatively large quantity of cyclohexene and oxidation proceeds selectively inside the pores of the support.

Generally, the reaction is believed to proceed through the mechanism postulated for Keggin type POMs. Monomeric, dimeric, and tetrameric peroxo species are generated by the reaction of polyoxometalates with hydrogen peroxide, and the peroxo species are supposed to be the active species for epoxidation of olefins within a POM/H_2O_2 system [42, 67, 72]. It has been postulated that the epoxidation reaction rate and epoxide yield, for the same type of catalytic species, are determined by the catalyst's acid strength [40, 73]. The lower activity of the PVMo/HMont, in comparison with PVMo catalyst, shows the importance of diffusional limitations. However the high diol selectivity with 20% PVMo/HMont is clearly justified considering the acidity of the support. The catalytic performance of the heterogeneous catalysts is also related to the fine dispersion of the active catalytic species within the supports. Here, the acid Brønsted sites of PVMo, acid Lewis sites of support and redox properties of PVMo are shown to have a crucial effect on the oxidation process. From table 3, it can also be seen that the catalytic activity of 20%PVMo-HMont is better than that of 10%PVMo-Hmont. The importance of the support has been also observed using HPAs immobilized in other supports, such as such as MCM-41 [24] SiO_2, SBA-15, ZrO_2-grafted SBA-15 [74].

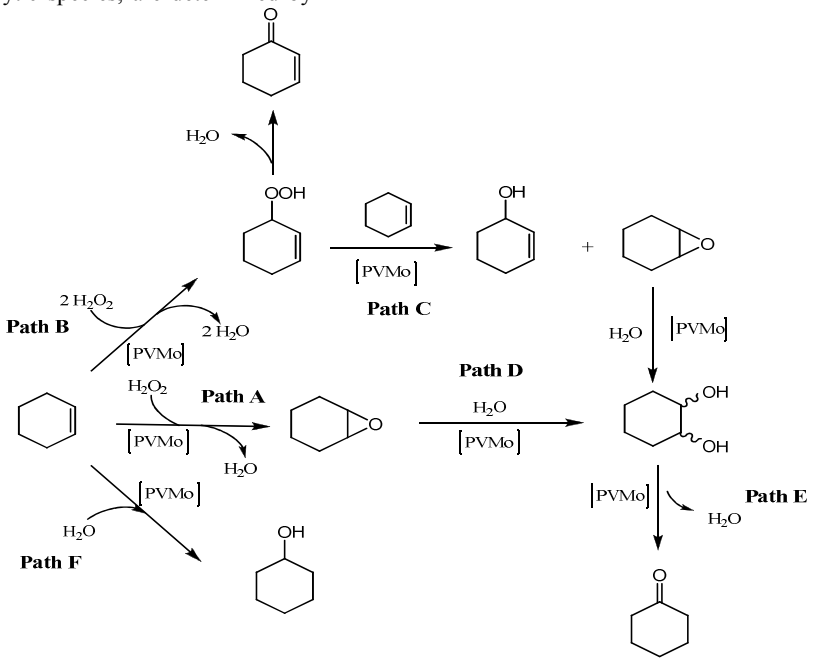

Fig. 8 Cyclohexene oxidation reaction products

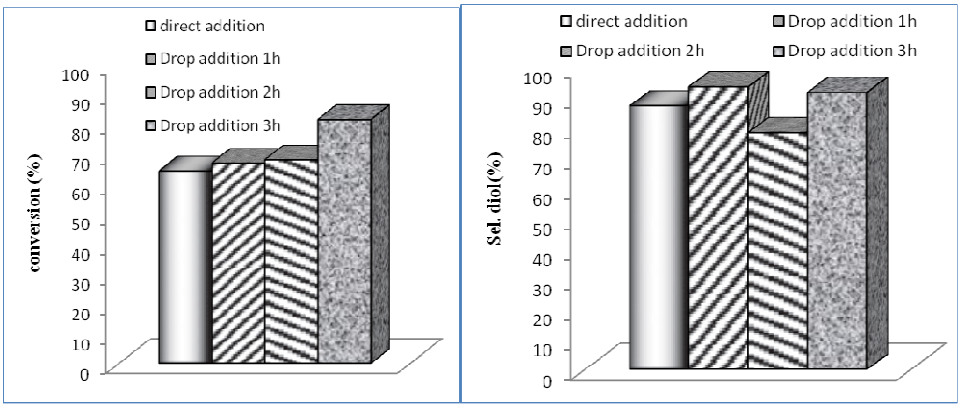

Fig. 9 The effect of addition type of H_2O_2 60% on the oxidation of cyclohexene (0.025 g catalyst 20%PVMo/HMont, 30 mmol cyclohexene, 30 mmol H_2O_2, 10 mL CH_3CN, 9 h of reaction, 70 ºC)

Table 3 Activity of various catalysts towards the oxidation of cyclohexene

Catalysts	Conversion (%)	Select. epoxide (%)	Select. Diol (%)	Select. allylic product (%)
HMont	28,5	-	-	-
PVMo	91,1	0.4	70,4	29.2
10%PVMo/HMont	70,6	16.9	36,8	46.3
20%PVMo/HMont	81,5	3.8	91,6	4.6

Reaction conditions: 0.025 g catalyst, 30 mmol cyclohexene, 30 mmol H_2O_2, 10 mL CH_3CN, 70 °C, 9 h.

Table 4 Effect of temperature on cyclohexene oxidation

Catalysts	Temperature /°C	Conversion /%	Sel. epoxide /%	Sel. diol /%	Sel. Allylic product /%
20%PVMo/HMont	40	24.2	3.1	61.5	35.4
	60	42.7	19.9	65.7	14.4
	70	81.5	3.8	91.6	4.6
	80	59.7	12.8	82.3	4.9
10%PVMo/HMont	60	33.5	31.8	33.3	39.9
	70	70.6	16.9	36.8	46.3
	80	51.4	4.6	72.3	23.1

Reaction conditions: 0.025 g catalyst, 30 mmol cyclohexene, 30 mmol H_2O_2, 10 mL CH_3CN, 9 h of reaction.

The comparison of the reaction at different temperatures (Table 4) so that, with both supported catalysts, best yields and selectivity's are reached at 70 ºC, both results are worse in reactions carried out at lower and higher temperatures.

A study was also carried out in order to see the effect of reaction time on the catalytic activity, with 0.025 g of catalyst, 30 mmol of cyclohexene, 30 mmol of hydrogen peroxide, 10 mL of acetonitrile, at the temperature 70 °C. The experimental results (Fig. 10) indicate that the reaction proceeds more slowly in the presence of heterogeneous catalysts. This may be attributed to diffusional restrictions of the reagents inside the pores of the catalyst.

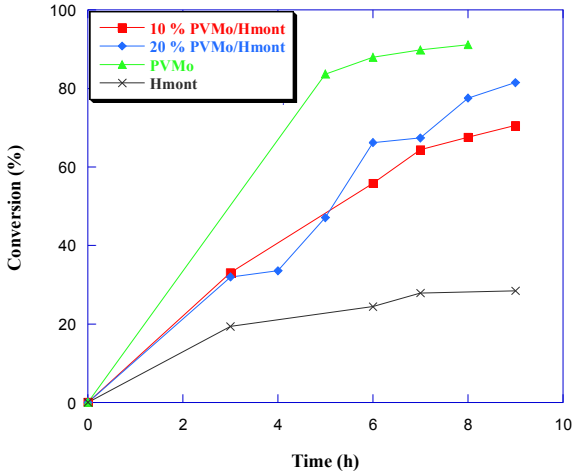

Fig. 10 Catalyst activity for cyclohexene oxidation.

The energy of activation was calculated using rate constant (*k*) determined at different temperatures. It is a well-established fact that in the oxidation of hydrocarbon, the rate of the reaction is proportional to the product concentration. The conversion vs time plots obtained in the present work indicate that the cyclohexene oxidation is not an exception to this fact.The reaction is considered to be second order with respect to the product and reactant concentration. The rate expression used by the many workers for oxidation reactions [2, 10, 11] is adopted here.

$$-d[cyclohexene]/d(t) = k[cyclohexene]^2 \quad (1)$$

on integrating expression (1), from the initial concentration at initial time to the final concentration at the final time t , the expression can be written as :

$$1/[cyclohexene] = 1[cyclohexene]_0 + k.t \quad (2)$$

A plot of $1/[cyclohexene]$ with respect to time gives a linear relationship showing a pseudo-second-order dependence on the cyclohexene, k represent the apparent rate constant. Fig. 11a shows this plot. All the points fall on a straight line which proves that the rate expression holds good under the conditions employed for the reaction in the present work.

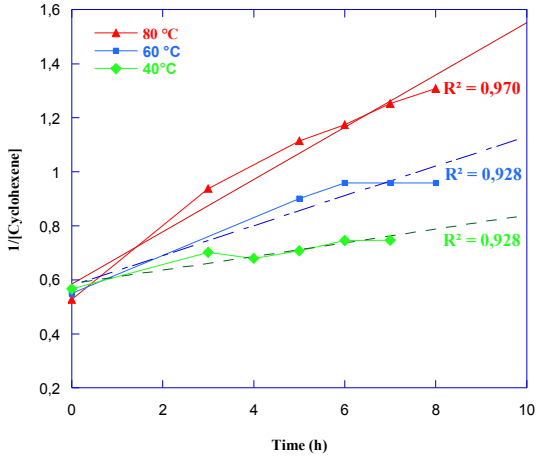

Fig. 11 a second-order kinetic plot for cyclohexene epoxidation with hydrogen peroxide over 20%PVMo-Hmont

Fig. 11b displays the graph of ln (*k)* obtained from expression (2) within 6 h versus the inverse of the reaction temperature for each temperature. The apparent activation energy (*E*a) calculated from the Arrhenius plot (Fig. 11b) was ca. 3.216 kcal mol^{-1}. K.C. Gupta et al and M. Abrantes et al [2, 3] reported the same apparent activation energy. However this value was low to the values reported in many works (Table 5).

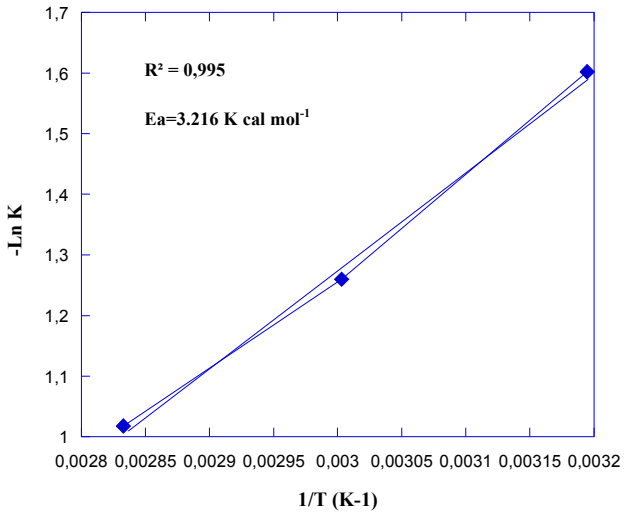

Fig. 11b Ln (apparent rate constant) vs. inverse of reaction temperature (Arrhenius plot of pseudo-first-order kinetics for epoxidation).

Table 5 E_a determined with different catalysts and different oxidants.

Catalyst	Oxidant	E_a (kcal mol^{-1})	Reference
MoO_2(SAL-SH.)DMF		25.8	4
Uncatalysed	O_2	20.6	75
MnO_2		13	76
Ru(III)-EDTA		8.6	77
Fe-HPHZ	H_2O_2	2.13	2
[(nBu$_3$Sn)$_2$*Mo*O$_4$]		5	3
PVMo-Hmont		3.21	Present work

Reaction conditions: 10 mL acetonitrile, 30 mmol cyclohexene, and 0.025 g catalyst, with H_2O_2/cyclohexene = 1.0. The reaction temperatures, are 40, 60, 70 and 80 °C, respectively.

3.3 Catalyst reusability

As the reusability of a catalyst is important from the economical and industrial points of view, we decided to investigate the reusability and stability of PVMo/Hmont in oxidation reactions. The catalysts were filtered and reused after 9 h of reaction time. They were washed for several times with a solvent, and then dried at room temperature and finally used in cyclohexene oxidation with a fresh reaction mixture. As a typical example, the catalyst 20% PVMo / Hmont showed (Fig. 12) a conversion of 81% in the first run, which decreased to about 61, 48 and 39 % in the 2nd, 3rd and 4th run, respectively. The amount of catalyst leaching after each run was determined by ICP analysis. In this manner, the filtrates were collected after each run and used to determine the amounts of leached vanadium (Table 6). The decrease in catalytic activity is due to the leaching of HPA (of about 1-2 %) from the support into the liquid phase during the catalytic reactions; this was confirmed by the well-known ascorbic acid test [75]. Although the catalyst was washed after filtration to remove all the adsorbed reactants and products, retention of some of the adsorbed reactants and products was still possible, and this might cause the blockage of active sites and consequently the decrease in the catalytic activity. The nature of the recovered catalyst was followed by FT-IR. After reusing the catalyst for several times, no change in the FT-IR spectrum was observed. However, the selectivity remained almost unchanged, and the catalysts were therefore reused four times.

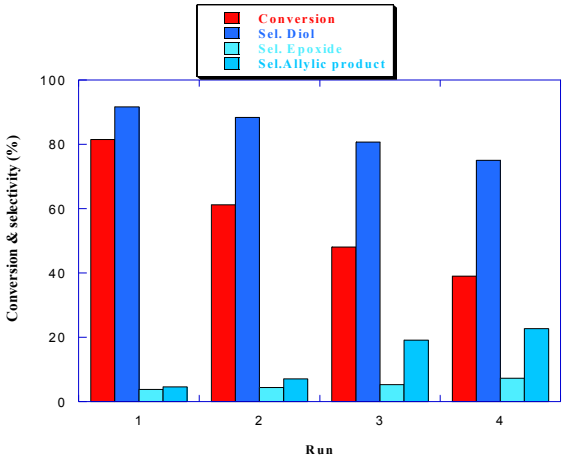

Fig.12 Reusability of 20% PVMo/Hmont on the oxidation of cyclohexene

Table 6 Vanadium leaching determined by ICP analysis

Run N°	1	2	3	4
Vanadium leaching (%)	1.9	1.8	1.4	1.3

4. Conclusion

In this work, we successfully prepared and characterized PVMo/HMont by a simple impregnation method. The XRF analysis showed that the procedure used gives the expected materials, and the PVMo structure is confirmed by ^{31}P NMR analysis. UV-Vis and IR bands show the Keggin structure of HPA. XRD analysis showed that PVMo is well dispersed on the surface of Montmorillonite. Thermal analysis showed that the material prepared is stable for temperatures up to 125 °C; this is explained by the formation of intermolecular bonds between PVMo and the support. The prepared heterogeneous catalysts showed high catalytic activity for cyclohexene epoxidation. They are not expensive and can be used in heterogeneous media. These catalysts showed that the reaction is oriented rather towards epoxides than enol. The use of a very small amount (25 mg) enabled to reach a good conversion (above 80 %) and yield of diol (about 77 %). The use of homogeneous catalyst PVMo gives only 64 % of diol. Also, using drop addition for 3 hours increased the conversion. H_2O_2 is a green and eco-friendly oxidant in these systems.

Acknowledgements

The authors would like to thank the General Directorate for Scientific Research and Technological Development (DGRST) as well as the Thematic Research Agency of Science and Technology (ATRST) for the financial support to the project PNR-8-U13-880.

References

1. Y. Liu, K. Murata, M. Inaba, H. Nakajima, M. Koya and K. Tomokuni, *Chem. Lett.*, 2004, **33**, 200-201.
2. R. A. Sheldon and J. Dakka, *Catal. Today*, 1994, **19**, 215-245.
3. D. Mandelli, M. C. A. van Vliet, R. A. Sheldon and U. Schuchardt, *Appl. Catal. A*, 2001, **219**, 209-213.
4. G. Centi and S. Perathoner, *Catal. Today*, 2003, **77**, 287-297.
5. K. A. Joergensen, *Chem. Rev.*, 1989, **89**, 431-458.
6. D. Hoegaerts, B. F. Sels, D. E. De Vos, F. Verpoort and P. A. Jacobs, *Catal. Today*, 2000, **60**, 209-218.
7. G. Grigoropoulou, J. H. Clark and J. A. Elings, *Green Chem.*, 2003, **5**, 1-7.
8. J.-M. Bregeault, *Dalton Transactions*, 2003, 3289-3302.
9. B. S. Lane and K. Burgess, *Chem. Rev.*, 2003, **103**, 2457-2474.
10. R. Noyori, M. Aoki and K. Sato, *Chem. Commun.*, 2003, 1977-1986.
11. K. Kamata, K. Yonehara, Y. Sumida, K. Yamaguchi, S. Hikichi and N. Mizuno, *Science*, 2003, **300**, 964-966.
12. F. Cavani, *Catal. Today*, 1998, **41**, 73-86.
13. F. Cavani and F. Trifiro, *Catal. Today*, 1999, **51**, 561-580.
14. I. V. Kozhevnikov, *Catal. Rev. Sci. Eng.*, 1995, **37**, 311-352.
15. M. Baerns and O. Buyevskaya, *Catal. Today*, 1998, **45**, 13-22.
16. M. Misono, *Catal. Rev. Sci. Eng.*, 1987, **29**, 269-321.
17. P. S. N. Rao, K. T. V. Rao, P. S. S. Prasad and N. Lingaiah, *Catal. Commun.*, 2010, **11**, 547-550.
18. K. I. Matveev, V. F. Odyakov and E. G. Zhizhina, *J. Mol. Catal. A*, 1996, **114**, 151-160.
19. S. Shinachi, M. Matsushita, K. Yamaguchi and N. Mizuno, *J. Catal.*, 2005, **233**, 81-89.
20. A. Sopa, A. Waclaw-Held, M. Grossy, J. Pijanka and K. Nowinska, *Appl. Catal. A*, 2005, **285**, 119-125.
21. D. P. Sawant, A. Vinu, J. Justus, P. Srinivasu and S. B. Halligudi, *J. Mol. Catal. A*, 2007, **276**, 150-157.
22. M. E. Chimienti, L. R. Pizzio, C. V. Caceres and M. N. Blanco, *Appl. Catal. A*, 2001, **208**, 7-19.
23. P. Sharma and A. Patel, *Appl. Surf. Sci.*, 2009, **255**, 7635-7641.
24. S. Tangestaninejad, V. Mirkhani, M. Moghadam, I. Mohammadpoor-Baltork, E. Shams and H. Salavati, *Ultrason. Sonchem.*, 2008, **15**, 438-447.
25. T. Ressler, U. Dorn, A. Walter, S. Schwarz and A. H. P. Hahn, *J. Catal.*, 2010, **275**, 1-10.
26. E. Rafiee, F. Shahbazi, M. Joshaghani and F. Tork, *J. Mol. Catal. A*, 2005, **242**, 129-134.
27. L. Chen, X. Wang, X. Guo, H. Guo, H. o. Liu and Y. Chen, *Chem. Eng. Sci.*, 2007, **62**, 4469-4478.
28. D. Mandelli, M. C. A. van Vliet, R. A. Sheldon and U. Schuchardt, *Applied Catalysis A: General*, 2001, **219**, 209-213.
29. S. K. Bhorodwaj and D. K. Dutta, *Appl. Catal. A*, 2010, **378**, 221-226.
30. O. S. Ahmed and D. K. Dutta, *J. Mol. Catal. A*, 2005, **229**, 227-231.
31. D. P. Sawant, A. Vinu, F. Lefebvre and S. B. Halligudi, *J. Mol. Catal. A*, 2007, **262**, 98-108.
32. M. P. Hart and D. R. Brown, *J. Mol. Catal. A*, 2004, **212**, 315-321.
33. G. D. Yadav and V. V. Bokade, *Appl. Catal. A*, 1996, **147**, 299-323.
34. R. Fazaeli and H. Aliyan, *Appl. Catal. A*, 2007, **331**, 78-83.
35. S. K. Bhorodwaj and D. K. Dutta, *Appl. Clay Sci.*, 2011, **53**, 347-352.
36. Z. Ding, J. T. Kloprogge, R. L. Frost, G. Q. Lu and H. Y. Zhu, *J. Pourous. Mater.*, 2001, **8**, 273-293.
37. C. H. Zhou, *Appl. Clay Sci.*, 2011, **53**, 87-96.
38. Z. W. Xi, H. P. Wang, Y. Sun, N. Zhou, G. Y. Cao and M. Li, *J. Mol. Catal. A*, 2001, **168**, 299-301.
39. Y. Ding, Q. Gao, G. X. Li, H. P. Zhang, J. M. Wang, L. Yan and J. S. Suo, *J. Mol. Catal. A*, 2004, **218**, 161-170.
40. J. M. Fraile, J. I. García, J. A. Mayoral and E. Vispe, *J. Catal.*, 2005, **233**, 90-99.
41. S. H. Jhung, J. H. Lee, A. K. Cheetham, G. Ferey and J. S. Chang, *J. Catal.*, 2006, **239**, 97-104.
42. Z. Weng, J. Wang, S. Zhang, C. Yan and X. Jian, *Appl. Catal. A*, 2008, **339**, 145-150.

43. M. Guidotti, C. Pirovano, N. Ravasio, B. Lazaro, J. M. Fraile, J. A. Mayoral, B. Coq and A. Galarneau, *Green Chem.*, 2009, **11**, 1421-1427.
44. H. Salavati, S. Tangestaninejad, M. Moghadam, V. Mirkhani and I. Mohammadpoor-Baltork, *Ultrason. Sonchem.*, 2010, **17**, 453-459.
45. H. Salavati and N. Rasouli, *Materials Research Bulletin*, 2011, **46**, 1853-1859.
46. A. C. Estrada, I. C. M. S. Santos, M. M. Q. Simoes, M. G. P. M. S. Neves, J. A. S. Cavaleiro and A. M. V. Cavaleiro, *Appl. Catal. A*, 2011, **392**, 28-35.
47. S. El-Korso, I. Rekkab, A. Choukchou-Braham, S. Bedrane, L. Pirault-Roy and C. Kappenstein, *Bull. Mater. Sci.*, 2012, **35**, 1187-1194.
48. D. Lahcene, A. Choukchou-Braham, C. Kappenstein and L. Pirault-Roy, *J. Sol Gel Sci. Tech.*, 2012, **64**, 637-642.
49. N. Ameur, S. Bedrane, R. Bachir and A. Choukchou-Braham, *J. Mol. Catal. A*, 2013, **374**, 1-6.
50. S. Bhattacharjee and J. A. Anderson, *J. Mol. Catal. A*, 2006, **249**, 103-110.
51. S. El-Korso, I. Khaldi, S. Bedrane, A. Choukchou-Braham, F. Thibault-Starzyk and R. Bachir, *J. Mol. Cat. A*, 2014, **394**, 89-96.
52. T. Ressler, O. Timpe, F. Girgsdies, J. Wienold and T. Neisius, *J. Catal.*, 2005, **231**, 279-291.
53. R. Mokaya and W. Jones, *J. Catal.*, 1995, **153**, 76-85.
54. K. Nowinska and W. Kaleta, *Appl. Catal. A*, 2000, **203**, 91-100.
55. A. Tarlani, M. Abedini, A. Nemati, M. Khabaz and M. M. Amini, *J. Coll. Inter. Sci.*, 2006, **303**, 32-38.
56. J. B. Condon, in *Surface Area and Porosity Determinations by Physisorption*, ed. J. B. Condon, Elsevier Science, Amsterdam, 2006, pp. 29-53.
57. J. B. Condon, in *Surface Area and Porosity Determinations by Physisorption*, ed. J. B. Condon, Elsevier Science, Amsterdam, 2006, pp. 55-90.
58. T. Mishra, K. M. Parida and S. B. Rao, *J. Coll. Inter. Sci.*, 1996, **183**, 176-183.
59. P. Villabrille, G. Romanelli, L. Gassa, P. Vazquez and C. Caceres, *Appl. Catal. A*, 2007, **324**, 69-76.
60. A. C. Garade, V. S. Kshirsagar, R. B. Mane, A. A. Ghalwadkar, U. D. Joshi and C. V. Rode, *Appl. Clay Sci.*, 2010, **48**, 164-170.
61. B. Li, Z. Liu, C. Han, J. Liu, S. Zuo, Z. Zhou and X. Pang, *J. Mol. Catal. A*, 2011, **348**, 106-113.
62. S. Benadji, P. Eloy, A. Leonard, B. L. Su, K. Bachari, C. Rabia and E. M. Gaigneaux, *Microp. Mesop. Mat.*, 2010, **130**, 103-114.
63. H. Salavati and N. Rasouli, *Appl. Surf. Sci.*, 2011, **257**, 4532-4538.
64. J. Zhang, Y. Tang, G. Y. Li and C. Hu, *Appl. Catal. A*, 2005, **278**, 251-261.
65. K. V. Bineesh, D.-K. Kim, M.-I. Kim and D.-W. Park, *Appl. Clay Sci.*, 2011, **53**, 204-211.
66. G. R. Rao and B. G. Mishra, *Mater. Chem. Phys.*, 2005, **89**, 110-115.
67. N. K. K. Raj, A. Ramaswamy and P. Manikandan, *J. Mol. Catal. A*, 2005, **227**, 37-45.
68. P. Villabrille, G. Romanelli, P. Vazquez and C. Caceres, *Appl. Catal. A*, 2004, **270**, 101-111.
69. S. Korichi, A. Elias, A. Mefti and A. Bensmaili, *Appl. Clay Sci.*, 2012, **59-60**, 76-83.
70. S. Dharne and V. V. Bokade, *J. Nat. Gas. Chem.*, 2011, **20**, 18-24.
71. G. B. B. Varadwaj, S. Rana and K. Parida, *Chem. Eng. J.*, 2013, **215**, 849-858.
72. C. Swalus, B. Farin, F. Gillard, M. Devillers and E. M. Gaigneaux, *Catal. Commun.*, 2013, **37**, 80-84.
73. Z. Karimi and A. R. Mahjoub, *Appl. Surf. Sci.*, 2010, **256**, 4473-4479.
74. F. Jing, B. Katryniok, E. Bordes-Richard and S. Paul, *Catal. Today*, 2013, **203**, 32-39.
75. G. D. Yadav and V. V. Bokade, *Appl. Catal. A*, 1996, **147**, 299-323.
76. H. J. Neuburg, M. J. Phillips and W. F. Graydon, *J. Catal.*, 1975, **38**, 33-46.
77. M. M. T. Khan and R. S. Shukla, *J. Mol. Catal.*, 1990, **58**, 405-413.

Heterogenization of homogenous catalysts consisting of vanadium substituted polyphosphomolybdate with Keggin structure supported on activated Bentonite for epoxidation of cyclohexene.

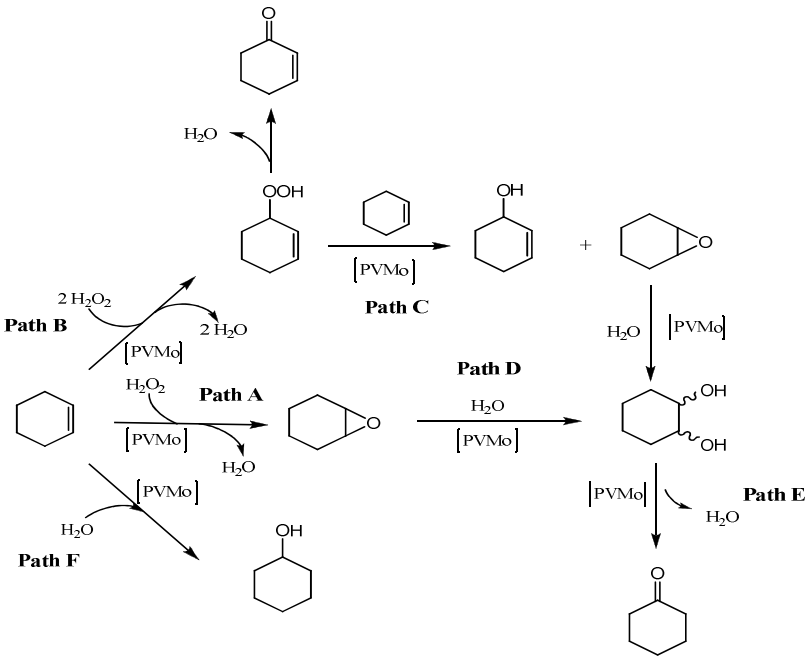

Graphical Abstract